chemosensors

MDPI

Communication

Online Measurement of Sodium Nitrite Based on Near-Infrared Spectroscopy

Xianzhe Xu †, Yongshen Zhang †, Mingmin Zhang, Dingming Li and Chen Zuo *

Institute of Radiochemistry, China Institute of Atomic Energy, Beijing 102413, China; xianzhexu_21@163.com (X.X.); m15110185336@163.com (Y.Z.); dingminglee@cnncmail.cn (D.L.)
* Correspondence: zchen_2008@126.com
† These authors contributed equally to this work.

Abstract: In this study, a method was developed for the rapid online measurement of sodium nitrite solutions using near-infrared spectroscopy. A series of standard solutions of sodium nitrite at different concentrations were prepared, and the samples were measured in cuvettes and flow cells. Following the preprocessing of raw spectra and band selection, partial least squares were used to establish a prediction model, and the coefficient of determination (R^2) of the validation set and the root mean square error of prediction (RMSEP) of the model were 0.9989 and 0.0338. The results demonstrate that the established model can meet the demands of online measurement and perform the rapid, nondestructive detection of sodium nitrite solutions, which provides some basis for the automated formulation of feedstock in spent fuel reprocessing.

Keywords: sodium nitrite; online measurement; near-infrared

Citation: Xu, X.; Zhang, Y.; Zhang, M.; Li, D.; Zuo, C. Online Measurement of Sodium Nitrite Based on Near-Infrared Spectroscopy. *Chemosensors* **2024**, *12*, 22. https://doi.org/10.3390/chemosensors12020022

Academic Editor: Frederic Melin

Received: 24 November 2023
Revised: 2 January 2024
Accepted: 25 January 2024
Published: 31 January 2024

1. Introduction

One of the central goals of reprocessing spent fuel is the recovery and purification of uranium and plutonium [1–4]. This process requires tuning uranium and plutonium valence states using reducing and oxidizing agents [5,6]. Among them, sodium nitrite is widely used in plutonium valence adjustment, and this reagent is often used to destroy the remaining reducing agent of the reaction. It needs to be prepared in large quantities when it is used, and for different parts of the process and different material concentrations, the concentration of sodium nitrite has different needs, generally in the range of 0.5–6 mol/L. If the reducing agent is prepared manually, it consumes a lot of manpower and time, so automated dosing is very necessary. And in automated dosing, besides the realization of automatic machine mixing, the online measurement of the product's concentration is also an important step.

There are many methods to determine the concentration of sodium nitrite [7], including spectrophotometry [8–10], chemiluminescence [11–13], electrochemistry [14–16], and chromatography [17–19], in addition to the conventional titration of chemical reagents. However, some of these methods are designed to detect trace concentrations. When higher concentrations of formulated products are detected, they must be diluted before being measured, making the process more cumbersome. However, many methods that allow higher concentration measurements require sample destruction and are challenging to measure online. In contrast, near-infrared (NIR) spectroscopy allows the faster and easier measurement of sodium nitrite at higher concentrations.

Refs. [20,21] show how NIR spectroscopy has recently been widely used in food processing [22], pharmaceutical manufacturing [23], and chemical product synthesis [24]. It has the advantage of rapid measurement without the loss of samples and is suitable for online measurement. NIR spectroscopy measures electromagnetic waves with wavelengths of 800–2500 nm. It is part of the multiplicative and combinatorial absorption spectra molecular vibrational spectroscopy [25], which mainly detects C-H, N-H, and O-H bonds in

samples [26], making them ideal for detecting organic matter. The vibration of the sample is shown in Figure 1. However, NIR spectroscopy can also detect inorganic substances, especially aqueous solutions. This is because the structure of water is susceptible to temperature and solute interactions. The presence of other ions in the sample affects the interaction between water molecules and alters the strength of hydrogen bonding, leading to changes in the near-infrared spectrum. The perturbation of water via temperature and electrolyte is linear [25,27–29], so aqueous solutions can be quantified using NIR.

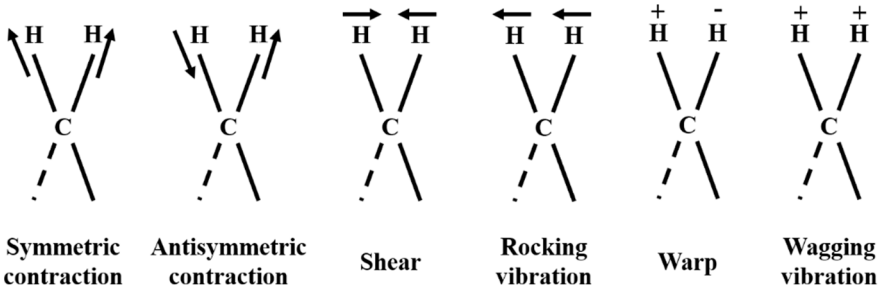

Figure 1. Example of the vibration of a sample ("+" indicates the vertical motion of the paper facing inward, "−" indicates the vertical motion of the paper facing outward).

In this study, a series of different concentrations of sodium nitrite solutions were measured, and an online measurement model of sodium nitrite was established and validated using flow samples with the aim of the rapid, nondestructive, and online detection of feedstock concentration in the automatic dosing of sodium nitrite.

2. Materials and Methods

2.1. Materials

The sodium nitrite used was purchased from Sinopharm Chemical Reagent Co., Ltd. (Shanghai, China) with a purity greater than 99.9%. The corresponding sodium nitrite was accurately weighed according to the concentration requirement and dissolved in deionized water with a resistivity of 18.2 MΩ·cm. The samples ranged from 0.3 to 6 mol/L, with a total of 43 concentrations, of which 33 samples were used for calibration and 10 samples were used for validation.

2.2. Instrumentation and Software

Spectroscopy was collected using a MATRIX-F NIR spectrometer (Bruker Optik GmbH, Saarbrücken, Germany).

Spectrum pretreatment and partial least squares modeling were performed using OPUS 8.5 spectral analysis software (Bruker).

2.3. Experimental Methods

The sample was placed in a quartz cuvette with an optical range of 2 mm for static samples. The experiment was conducted with an air background, with a scanning range of 12,000 to 4000 cm^{-1} and a resolution of 4 cm^{-1}. The scan time was 32 scans, and each concentration was measured at least twice.

For flow samples, the sample was placed in a beaker, and a flow pump was used to circulate the liquid between the beaker and the flow cell; the optical range of the flow cell was 2 mm, the flow pump speed was 50 mL/min, and the other test conditions were the same as those for static samples. A simple schematic of the online device is shown below (Figure 2).

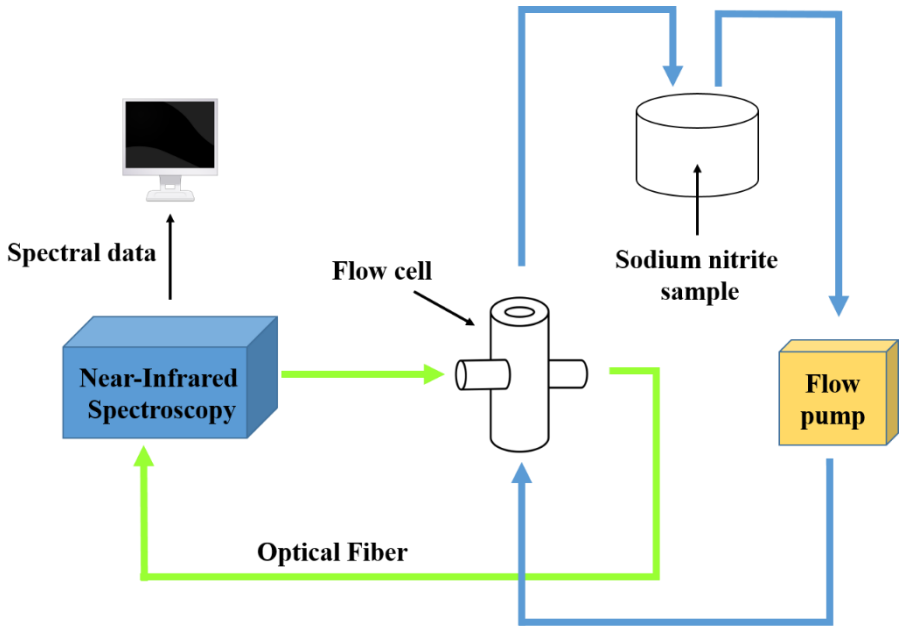

Figure 2. Schematic diagram of online device.

2.4. Pretreatment of Spectral Data

Spectral pretreatment is needed before modeling to make the quantitative model more accurate and stable. The preprocessing methods used include eliminating constant offsets, subtracting a straight line, max–min normalization, multiple scattering corrections, vector normalization, first-order and second-order derivatives, and combinations of these methods. The results of the different preprocessing methods were compared, and the optimal combination was selected for modeling.

2.5. Model Alignment

A partial least squares method established a prediction model based on the NIR spectra of a sodium nitrite standard solution. The partial least squares method is a classical linear modeling method commonly used in NIR ranges quantitative analysis. It has the advantages of noise cancellation, comprehensive spectrum data screening, and the complete extraction of adequate spectral information. The reasonableness of the model is further evaluated using the deterministic coefficient (R^2), root mean square error of cross-validation (RMSECV), and root mean square error of prediction (RMSEP).

3. Results and Discussion

3.1. NIR Spectrum Characteristics

The scanning range of spectra selected was 12,000–4000 cm^{-1}, and the raw spectra of several typical concentration samples are shown in Figure 3. In the raw spectra, a significant variation in the absorbance intensity and the concentration of sample wave number from 4250 to 4800 cm^{-1} and 5400 to 7100 cm^{-1} was observed in relation to the O-H bond. Among them, the strong absorption peak near 6900 cm^{-1} was due to the symmetric and antisymmetric stretching vibration (ν1 + ν3) of the O-H bond of water. In contrast, the weak absorption peak near 5600 cm^{-1} comprised the bending vibration of the O-H bond and the antisymmetric stretching vibration (ν2 + ν3) [30,31]. As for 4250–4800 cm^{-1}, this part of the absorption band was the firm absorption peaks of the adjacent two of the wave valleys. The strong absorption peak at 5100 cm^{-1}, which consists of a combination of three vibrational modes of the O-H bond, was unsuitable for use in the model because its intensity was too high. Since the power of O-H was affected by the concentration of the sample, the difference in the intensity of these absorption peaks indirectly reflected the difference in the attention of the sample. Although the differences between the spectra are evident, the

spectra overlap and are disturbed by the background, requiring the preprocessing of the original spectra to make the resulting models more accurate.

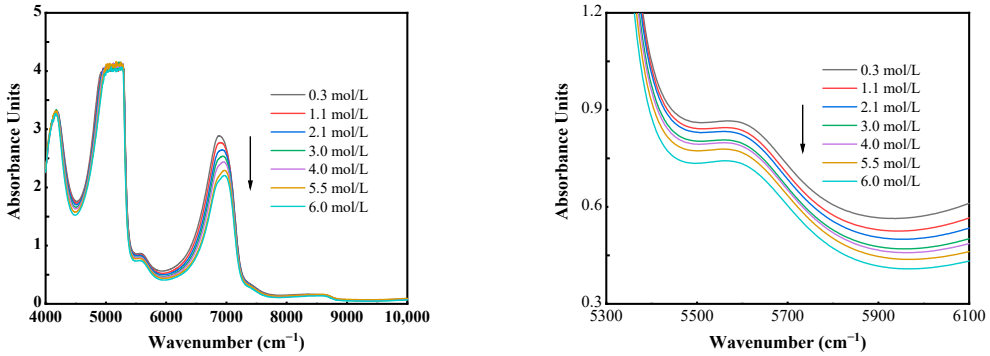

Figure 3. Near-infrared spectra of different concentrations of sodium nitrite.

3.2. Screening of Preprocessing Methods

To reduce the interference information unrelated to the chemical composition of the sample, the original spectrum of the sample was pretreated to make the final analysis result more accurate. With a uniformly selected spectral band of 5400–7500 cm^{-1} for modeling, 11 different spectral preprocessing methods were used in this study to process the raw spectra. Comparisons of the corresponding sodium nitrite concentration prediction models are shown in Table 1. The results from R^2 and RMSECV show that the best method was the multivariate scattering correction with 1.0000 and 0.0105 results, followed by vector normalization with 1.0000 and 0.0116 results, and the worst method was the second derivative with 0.9992 and 0.0454 results.

Table 1. Results of raw spectra after different pre-processing methods.

Number	Preprocessing Method	Wave Number (cm^{-1})	R^2	RMSECV
1	No spectral pretreatment	5400–7500	0.9999	0.0145
2	**eliminating constant offset**	5400–7500	0.9999	0.0197
3	**subtracting a straight line**	5400–7500	0.9999	0.0163
4	**vector normalization**	5400–7500	1.0000	0.0116
5	**max–min normalization**	5400–7500	1.0000	0.0122
6	**multiple scattering correction** (MSC)	5400–7500	1.0000	0.0105
7	First-order derivative	5400–7500	0.9999	0.0224
8	Second-order derivative	5400–7500	0.9992	0.0454
9	First-order derivative + **subtracting a straight line**	5400–7500	0.9999	0.0217
10	First-order derivative + **vector normalization**	5400–7500	0.9999	0.0208
11	First-order derivative + MSC	5400–7500	0.9999	0.0217

3.3. Spectrum Band Selection

Following the identification of models using multiple scattering correction methods, the bands used for spectroscopy were optimized, and a total of 24 rounds were tested, as shown in Table 2 below. The band with the best model predictions was 5450–7500 cm^{-1}, when the RMSECV value was the smallest, with a result of 0.0104, followed by 4250–4600 cm^{-1} and 5450–7500 cm^{-1}, when the RMSECV value was 0.0106.

Table 2. The effect of choosing different bands on modeling.

Number	Wave Number (cm^{-1})	RMSECV
1	5450–9400	0.0110
2	4250–4600, 6100–7500	0.0121
3	4250–4600, 5400–9400	0.0130
4	4250–4600, 5450–7500	0.0106
5	4250–4600, 6100–9400	0.0171
6	5450–7426	0.0109
7	5450–7500	0.0104
8	6100–7500	0.0204
9	6100–9400	0.0193
10	4250–4600, 5450–6100, 7500–9400	0.0125
11	4250–4600, 7500–9400	0.0250
12	5450–6100	0.0119
13	5450–6100, 7500–9400	0.0113
14	7424–9400	0.0114
15	4600–9400	0.0215
16	7500–9400	0.0205
17	4250–9400	0.0208
18	4250–5450, 6100–7500	0.0389
19	4600–7500	0.0318
20	4600–5450, 6100–7500	0.0403
21	4250–4600, 5450–6100	0.0203
22	4250–7500	0.0280
23	4250–5450, 6100–9400	0.0445
24	4600–5450, 6100–9400	0.0449

3.4. Identification of Latent Varying Numbers

After determining the optimal frequency band of the model, the latent varying numbers of the model were optimized. When the latent varying numbers were too small, the match between the model and the training set was not good enough to make full use of the adequate information of the spectrum; when the latent variable numbers were too large, the model could overfit the training set, and the resulting model would have a significant deviation in the subsequent validation process. In this study, the RSMECV values of models with different latent variable numbers were used to measure the adequacy of the number of latent varying numbers, as shown in Figure 4. The model had the smallest RSMECV value of 0.0104 when the latent variable number was 5. As the latent variable number increased or decreased from five, the RSMECV value of the model increased to more than 0.011.

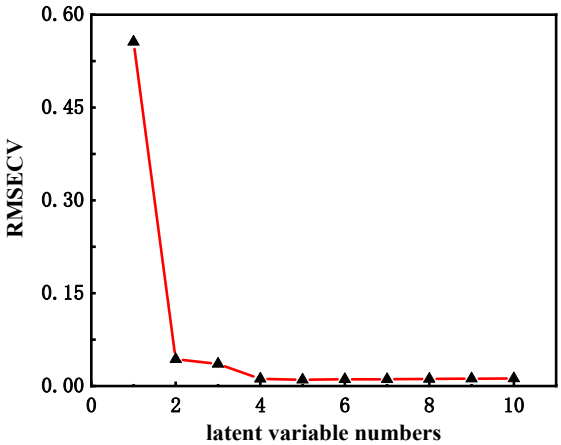

Figure 4. RSMECV plots for different latent varying number models.

3.5. Validation of Predictive Models

Spectra of 10 samples with different concentrations of sodium nitrite were measured, containing both stationary and flowing samples. The spectra were predicted using the model developed, and the results of the prediction and evaluation are shown in Figure 5 below, with specific data in Supplementary Table S1, where 1–24 are flowing samples, and 25–30 are stationary samples.

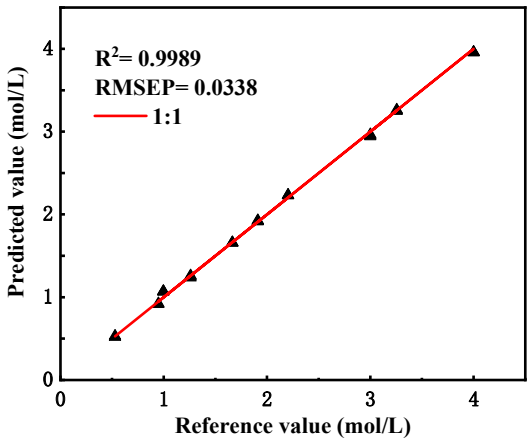

Figure 5. Predictions and assessment results of the sodium nitrite model.

After calculation, the R^2 value of the model validation set was 0.9955, and the RMSEP value was 0.0707. The results show that the model predictions are more reliable for stationary samples, but for flowing samples, some are better predicted, and some are poorly predicted.

3.6. Predicted Results of the Modified Model

The prediction results in Section 3.5 show that the established spectral model still has some defects; for stationary samples, the model was able to measure the sample concentration more accurately, while for flowing samples, some of the predictions were poor, so some of the predicted results that were close to the true value were not credible enough. There may be many reasons for this deviation, such as the tiny bubbles that may exist in the pipeline when flowing and the effect of the liquid's own flow on the spectra. Therefore, the spectra of four different concentrations of sodium nitrite flow samples were additionally collected and added to the model for correction, and the model was processed in the same way as Sections 3.2–3.4. The results can be seen in the Supplementary Tables S2 and S3 and Supplementary Figure S1. The corrected model, whose pre-processing method is still the multivariate scattering correction method, changed the optimal spectral band of choice to 5450–7426 cm^{-1}, and the number of factors remained unchanged.

The existing spectra were re-predicted using the new model, and the predicted results are shown in Figure 6 below, with specific data in Supplementary Data Table S4.

After calculation, the R^2 value of the model validation set was 0.9989, and the RMSEP value was 0.0338. The results show that after correction, the predictive ability of the model for stationary spectra decreased, but the relative error was still not higher than 2%, which still met the practical needs, while the predictive ability of the flow spectra was significantly improved, and the magnitude of the error value was significantly reduced.

In addition, some concentration samples were selected for longer online tests, and the results are shown in Figure 7 below. After calculation, the relative deviation of the predicted value of the samples compared with the mean value was generally below 1%, the deviation of the samples increased occasionally, and its relative deviation was at the maximum near 4%. Overall, the fluctuation of the predicted value of the samples in the continuous test was relatively small, and it could be basically kept unchanged and satisfy the demand for online measurement.

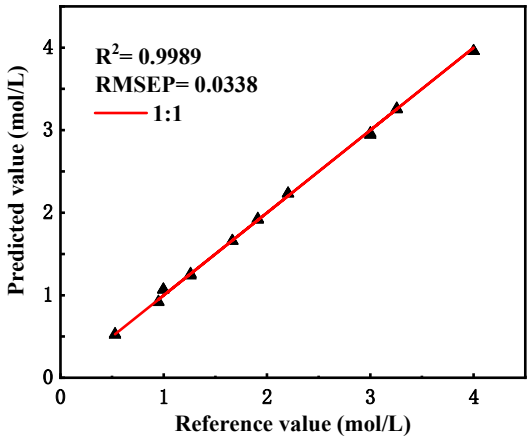

Figure 6. Predictions and assessment results of the modified model.

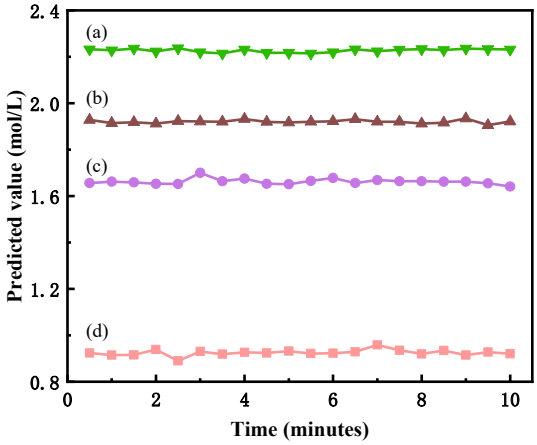

Figure 7. Long-time online measurement results of different concentration samples. (a) 0.949 mol/L, (b) 1.665 mol/L, (c) 1.910 mol/L, (d) 2.204 mol/L.

4. Conclusions

This work established an online measurement model of sodium nitrite based on NIR spectroscopy. The experimental results show that reasonable spectral pretreatment and appropriate band selection can improve the model's prediction ability. After testing, the final choice is to use the method of multiple scattering corrections to preprocess the raw spectra, and the method of modeling is the partial least squares method. The selected bands are 5450–7426 cm^{-1}. The spectral prediction of the online sodium nitrite model was good, with an R^2 value of 0.9989 and an RMSEP value of 0.0338. The relative deviation of the samples is small, the spectral measurement is relatively stable, and the prediction results of the model can be kept basically constant for a long period of time so that it can meet the demand for the online concentration measurement of sodium nitrite, and it provides support for automated sodium nitrite preparation in the factory.

Supplementary Materials: The following supporting information can be downloaded at: https://www.mdpi.com/article/10.3390/chemosensors12020022/s1, Figure S1: Results of the calibrated model selecting different number of factors; Table S1: Predictions and assessment results of the sodium nitrite model; Table S2: Results of different spectral preprocessing methods selected for the calibrated model; Table S3: Results of the calibrated model selecting different spectral bands; Table S4: Predictions and assessment results of the modified model; Table S5: Reference values for samples used for calibration and prediction.

Author Contributions: Conceptualization, Y.Z.; Methodology, X.X., D.L. and Y.Z.; Software, X.X.; Validation, X.X. and M.Z.; Formal analysis, X.X.; Investigation, X.X.; Resources, Y.Z.; Data curation, X.X.; Writing—original draft preparation, X.X.; Writing—review and editing, C.Z. and D.L.; Supervision, D.L.; Experimental, X.X., C.Z. and M.Z. All authors have read and agreed to the published version of the manuscript.

Funding: Research was supported by the China Atomic Energy Agency through the Program BG17000703 and was performed at the China Institute of Atomic Energy (CIAE).

Institutional Review Board Statement: Not applicable.

Informed Consent Statement: Not applicable.

Data Availability Statement: The data used to support the findings of this study are available from the corresponding author upon request.

Conflicts of Interest: The authors declare no conflicts of interest.

References

1. Moratilla Soria, B.Y.; Uris Mas, M.; Estadieu, M.; Villar Lejarreta, A.; Echevarria-López, D. Recycling versus Long-Term Storage of Nuclear Fuel: Economic Factors. *Sci. Technol. Nucl. Install.* **2013**, *2013*, 417048. [CrossRef]
2. Kumari, I.; Kumar, B.V.R.; Khanna, A. A review on UREX processes for nuclear spent fuel reprocessing. *Nucl. Eng. Des.* **2020**, *358*, 110410. [CrossRef]
3. Rodríguez-Penalonga, L.; Moratilla Soria, B.Y. A Review of the Nuclear Fuel Cycle Strategies and the Spent Nuclear Fuel Management Technologies. *Energies* **2017**, *10*, 1235. [CrossRef]
4. Ye, G.A.; Zhang, H. A Review on the Development of Spent Nuclear Fuel Reprocessing and Its Related Radiochemistry. *Prog. Chem.* **2011**, *23*, 1289–1294.
5. Fox, O.D.; Jones, C.J.; Birkett, J.E.; Carrott, M.J.; Crooks, G.; Maher, C.J.; Roube, C.V.; Taylor, R.J. Advanced PUREX Flowsheets for Future Np and Pu Fuel Cycle Demands. In *Separations for the Nuclear Fuel Cycle in the 21st Century*; Lumetta, G.J., Nash, K.L., Clark, S.B., Friese, J.I., Eds.; ACS Symposium Series; ACS: London, UK, 2006; Volume 933, pp. 89–102.
6. Paiva, A.P.; Malik, P. Recent advances on the chemistry of solvent extraction applied to the reprocessing of spent nuclear fuels and radioactive wastes. *J. Radioanal. Nucl. Chem.* **2004**, *261*, 485–496. [CrossRef]
7. Wang, Q.-H.; Yu, L.-J.; Liu, Y.; Lin, L.; Lu, R.-g.; Zhu, J.-p.; He, L.; Lu, Z.-L. Methods for the detection and determination of nitrite and nitrate: A review. *Talanta* **2017**, *165*, 709–720. [CrossRef] [PubMed]
8. Ensafi, A.A.; Amini, M. A highly selective optical sensor for catalytic determination of ultra-trace amounts of nitrite in water and foods based on brilliant cresyl blue as a sensing reagent. *Sens. Actuators B-Chem.* **2010**, *147*, 61–66. [CrossRef]
9. Tsikas, D. Analysis of nitrite and nitrate in biological fluids by assays based on the Griess reaction: Appraisal of the Griess reaction in the L-arginine/nitric oxide area of research. *J. Chromatogr. B-Anal. Technol. Biomed. Life Sci.* **2007**, *851*, 51–70. [CrossRef] [PubMed]
10. Moldovan, Z. Kinetic Spectrophotometric Determination of Nitrite with Tropaeolin 00-Bromate System. *Anal. Lett.* **2010**, *43*, 1344–1354. [CrossRef]
11. Lin, Z.; Xue, W.; Chen, H.; Lin, J.M. Peroxynitrous-Acid-Induced Chemiluminescence of Fluorescent Carbon Dots for Nitrite Sensing. *Anal. Chem.* **2011**, *83*, 8245–8251. [CrossRef]
12. Yaqoob, M.; Biot, B.F.; Nabi, A.; Worsfold, P.J. Determination of nitrate and nitrite in freshwaters using flow-injection with luminol chemiluminescence detection. *Luminescence* **2012**, *27*, 419–425. [CrossRef]
13. Nagababu, E.; Rifkind, J.M. Measurement of plasma nitrite by chemiluminescence without interference of S-, N-nitroso and nitrated species. *Free. Radic. Biol. Med.* **2007**, *42*, 1146–1154. [CrossRef]
14. Kozub, B.R.; Rees, N.V.; Compton, R.G. Electrochemical determination of nitrite at a bare glassy carbon electrode; why chemically modify electrodes? *Sens. Actuators B-Chem.* **2010**, *143*, 539–546. [CrossRef]
15. Zhu, N.; Xu, Q.; Li, S.; Gao, H. Electrochemical determination of nitrite based on poly(amidoamine) dendrimer-modified carbon nanotubes for nitrite oxidation. *Electrochem. Commun.* **2009**, *11*, 2308–2311. [CrossRef]
16. Kalimuthu, P.; John, S.A. Highly sensitive and selective amperometric determination of nitrite using electropolymerized film of functionalized thiadiazole modified glassy carbon electrode. *Electrochem. Commun.* **2009**, *11*, 1065–1068. [CrossRef]
17. Kodamatani, H.; Yamazaki, S.; Saito, K.; Tomiyasu, T.; Komatsu, Y. Selective determination method for measurement of nitrite and nitrate in water samples using high-performance liquid chromatography with post-column photochemical reaction and chemiluminescence detection. *J. Chromatogr. A* **2009**, *1216*, 3163–3167. [CrossRef] [PubMed]
18. Butt, S.B.; Riaz, M.; Iqbal, M.Z. Simultaneous determination of nitrite and nitrate by normal phase ion-pair liquid chromatography. *Talanta* **2001**, *55*, 789–797. [CrossRef] [PubMed]
19. Zuo, Y.; Wang, C.; Van, T. Simultaneous determination of nitrite and nitrate in dew, rain, snow and lake water samples by ion-pair high-performance liquid chromatography. *Talanta* **2006**, *70*, 281–285. [CrossRef] [PubMed]

20. Pasquini, C. Near infrared spectroscopy: A mature analytical technique with new perspectives—A review. *Anal. Chim. Acta* **2018**, *1026*, 8–36. [CrossRef] [PubMed]
21. Chu, X.L.; Xu, Y.P.; Lu, W.Z. Research and application progress of chemometrics methods in near infrared spectroscopic analysis. *Chin. J. Anal. Chem.* **2008**, *36*, 702–709.
22. Borras, E.; Ferre, J.; Boque, R.; Mestres, M.; Acena, L.; Busto, O. Data fusion methodologies for food and beverage authentication and quality assessment—A review. *Anal. Chim. Acta* **2015**, *891*, 1–14. [CrossRef] [PubMed]
23. Gad, H.A.; El-Ahmady, S.H.; Abou-Shoer, M.I.; Al-Azizi, M.M. Application of Chemometrics in Authentication of Herbal Medicines: A Review. *Phytochem. Anal.* **2013**, *24*, 1–24. [CrossRef]
24. Chung, H. Applications of near-infrared spectroscopy in refineries and important issues to address. *Appl. Spectrosc. Rev.* **2007**, *42*, 251–285. [CrossRef]
25. Wenz, J.J. Examining water in model membranes by near infrared spectroscopy and multivariate analysis. *Biochim. Biophys. Acta Biomembr.* **2018**, *1860*, 673–682. [CrossRef] [PubMed]
26. Sadergaski, L.R.; Irvine, S.B.; Andrews, H.B. Partial Least Squares, Experimental Design, and Near-Infrared Spectrophotometry for the Remote Quantification of Nitric Acid Concentration and Temperature. *Molecules* **2023**, *28*, 3224. [CrossRef] [PubMed]
27. Lin, J.; Brown, C.W. Near-IR spectroscopic measurement of seawater salinity. *Environ. Sci. Technol.* **2002**, *27*, 1611–1615. [CrossRef]
28. Sadergaski, L.R.; Toney, G.K.; Delmau, L.H.; Myhre, K.G. Chemometrics and Experimental Design for the Quantification of Nitrate Salts in Nitric Acid: Near-Infrared Spectroscopy Absorption Analysis. *Appl. Spectrosc.* **2021**, *75*, 1155–1167. [CrossRef]
29. Espinoza, L.H.; Lucas, D.; Littlejohn, D. Characterization of Hazardous Aqueous Samples by Near-IR Spectroscopy. *Appl. Spectrosc.* **2016**, *53*, 97–102. [CrossRef]
30. Murayama, K.; Ozaki, Y. Two-dimensional near-IR correlation spectroscopy study of molten globule-like state of ovalbumin in acidic pH region: Simultaneous changes in hydration and secondary structure. *Biopolymers* **2002**, *67*, 394–405. [CrossRef]
31. Maeda, H.; Ozaki, Y.; Tanaka, M.; Hayashi, N.; Kojima, T. Near Infrared Spectroscopy and Chemometrics Studies of Temperature-Dependent Spectral Variations of Water: Relationship between Spectral Changes and Hydrogen Bonds. *J. Near Infrared Spectrosc.* **2017**, *3*, 191–201. [CrossRef]